

# Voronoi Diagrams for Page Segmentation

Marina Gardella<sup>1</sup>, Ignacio Ramirez<sup>2</sup>

<sup>1</sup>Université Paris-Saclay, ENS Paris-Saclay, Centre Borelli, Gif-sur-Yvette, France

<sup>2</sup>IIE, Facultad de Ingeniería, Universidad de la República, Uruguay

[marina.gardella@impa.br](mailto:marina.gardella@impa.br), [nacho@fing.edu.uy](mailto:nacho@fing.edu.uy)

*Communicated by* Seginus Mowlavi and Antoine Tadros      *Demo edited by* Marina Gardella

## Abstract

Page segmentation is a key task in document processing, enabling effective extraction of structured information from diverse document types. This paper presents an in-depth analysis of the method proposed by Kise et al., a bottom-up approach using area Voronoi diagrams to identify spatial relationships between document parts. Our work provides a detailed description of the method, emphasizing clarity, reproducibility, and transparency, particularly regarding aspects not fully specified in the original paper. We highlight the impact of the parameter settings and preprocessing steps on the method's performance. Through extensive testing, we demonstrate that the method can handle a wide range of layouts but exhibits notable sensitivity to specific document characteristics, especially in handling complex elements like handwritten text, lists, drop-caps, and tables.

## Source Code

The reviewed source code and documentation for this algorithm are available from the web page of this article<sup>1</sup>. Usage instructions are included in the `README.md` file of the archive.

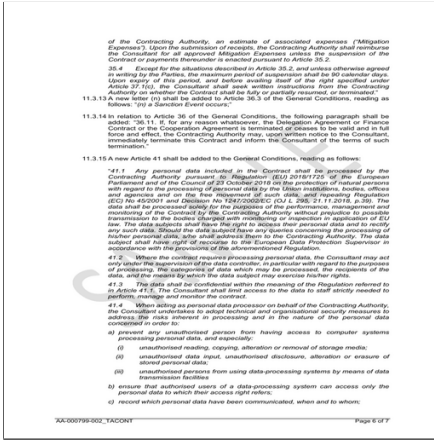
**Keywords:** document layout analysis; Voronoi diagram

## 1 Introduction

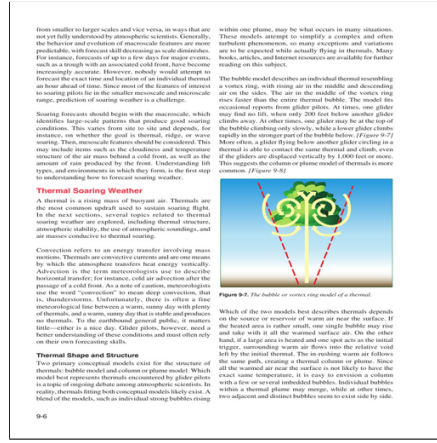
Document layout analysis is crucial in the field of document processing, as it enables systems to extract meaningful information from diverse types of documents. Page segmentation, in particular, plays a pivotal role in this process by dividing a page into distinct regions, such as text blocks, images, tables, and headers. Accurate segmentation is essential for enabling downstream tasks like optical character recognition (OCR), content extraction, and layout reconstruction, ensuring that different elements are appropriately interpreted.

Document layouts can vary significantly depending on the structure and formatting of the content, making page segmentation a challenging task. Some documents exhibit non-overlapping layouts

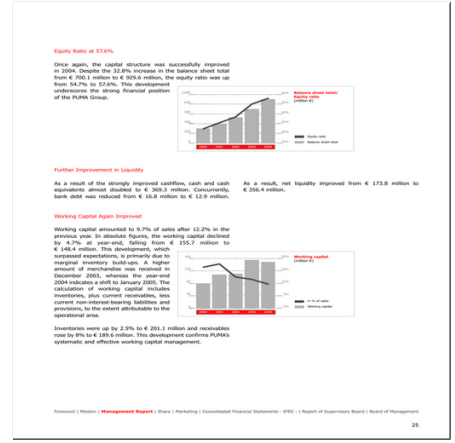
<sup>1</sup><https://doi.org/10.5201/ipol.2026.591>



(a) Overlapping Layout



(b) Manhattan Layout



(c) Non-Manhattan Layout

Figure 1: Examples of documents with different layouts. The document in Figure 1a presents overlapping elements: a stamp overlaps the text. The document in Figure 1b has a Manhattan layout: document parts have rectangular boundaries. In contrast, the document in Figure 1c involves irregular boundaries, following a non-Manhattan layout.

where content blocks, such as text and images, are distinctly separated. More complex documents may include overlapping regions where, for instance, text may flow over images or stamps may appear over the text. Figure 1a shows an example of an overlapping layout. In terms of geometric structure, the so-called *Manhattan layouts* follow rectangular divisions, which are common in standard forms or structured documents, as shown in Figure 1b. Non-Manhattan layouts, often found in more visually dynamic documents like magazines or presentations, involve irregular or slanted boundaries. Such a layout is depicted in Figure 1c.

Various strategies have been developed to handle page segmentation effectively, each with its own strengths and weaknesses. Bottom-up approaches [8, 9] start with small components, such as connected pixels or characters, and progressively group them into larger structures like words, lines, and paragraphs, based on spatial proximity or similarity. Conversely, top-down approaches [4, 6] begin by dividing the page into large regions, which are then recursively split until the desired level of granularity is achieved (lines, words, characters). Hybrid methods [13, 12] combine elements of both strategies to leverage their respective advantages, offering more flexibility in handling diverse layouts. Finally, there are holistic approaches that attempt to infer the whole structure of the document in one shot. Recent methods based on deep learning [3, 2, 5, 14, 15] belong to this category. These methods rely on learning their task from large amounts of labeled data, which has become increasingly available [11, 16].

This work describes and provides an implementation of the method developed by Kise et al. [8] that is as faithful as possible to the original. This method is a bottom-up approach which uses the so called *Area Voronoi Diagram* of the connected components of the image as an auxiliary data structure for determining the spatial relationship between such components. In describing the method, we focus on clarity of presentation, unambiguous definitions, and total transparency regarding the aspects that are either not fully described in the original paper, or which may have a relevant influence on the performance of the method, such as thresholds, parameters, etc. As for the implementation, we provide a clear, concise, and thoroughly documented implementation with a rich command-line interface. The code can be run as a Python-only implementation, which is readily portable.

## 2 Voronoi Diagrams

Computational geometry is a branch of computer science that deals with the study and development of algorithms for solving geometric problems. This field often emerges in response to challenges found in image processing and pattern recognition, where the inherent geometry of visual data needs to be analyzed, understood, and manipulated. Among the many tools of computational geometry, Voronoi diagrams are particularly significant, as they arise as a natural partitioning of the space [1]. In this section, we shall review the main concepts of Voronoi diagrams.

### 2.1 Point Voronoi Diagram

Let  $P = \{p_1, \dots, p_n\} \subset \mathbb{R}^2$  be a set of points, which we shall refer to as *generators*. The *Voronoi region* associated with  $p_i$  is the set of points that are closer to  $p_i$  than to any other point in  $P$ . Formally, the Voronoi region associated with  $p_i$  is given by

$$\mathfrak{v}(p_i) = \{p : d(p, p_i) \leq d(p, p_j), \text{ for all } j \neq i\} = \bigcap_{j \neq i} \{p : d(p, p_i) \leq d(p, p_j)\}, \quad (1)$$

where  $d$  denotes the Euclidean or  $l_2$  distance. According to Equation (1), each Voronoi region is an intersection of half-planes, that is, a convex polygon. The boundaries of such regions are line segments, half-line segments, or infinite lines, which we shall refer to as *Voronoi ridges*<sup>2</sup> and we shall refer to their endpoints as *Voronoi vertices*. Finally, the *Point Voronoi Diagram* associated with the set of generators  $P$  is the set of Voronoi regions associated with each point in  $P$

$$\mathcal{V}(P) = \{\mathfrak{v}(p_1), \dots, \mathfrak{v}(p_n)\}. \quad (2)$$

### 2.2 Area Voronoi Diagram

Point Voronoi diagrams define regions according to the distance to a set of isolated points. This idea can be generalized to distances to a set of regions of connected points, which we call *components*. Consider  $C = \{c_1, \dots, c_n\}$  a set of non-overlapping components in  $\mathbb{R}^2$ , and  $d(p, c_r)$  the distance between a point  $p \in \mathbb{R}^2$  and a component  $c_r$ , defined as the shortest Euclidean distance from  $p$  to any point in  $c_r$ . Analogous to the previous case, the Voronoi region associated with  $c_r$  is the set of points that are closer to  $c_r$  than to any other component in  $C$

$$\mathfrak{v}(c_r) = \{p \text{ such that } d(p, c_r) \leq d(p, c_l), \text{ for all } l \neq r\}. \quad (3)$$

Analogous to the Point Voronoi Diagram, the *Area Voronoi Diagram* associated with  $C$  is the set of Voronoi regions associated with each component in  $C$

$$\mathcal{V}(C) = \{\mathfrak{v}(c_1), \dots, \mathfrak{v}(c_n)\}. \quad (4)$$

### 2.3 Approximate Area Voronoi Diagram

Computing exact Area Voronoi diagrams can be computationally expensive. However, they can be approximated using the Point Voronoi Diagram. Such a construction involves three steps:

1. For each component  $c_i$ , sample points along its boundary  $P_{c_i} = \{p_1^{c_i}, \dots, p_{n_{c_i}}^{c_i}\}$ .

---

<sup>2</sup>The original paper refers to these as *Voronoi edges*. We choose to keep the terminology used in the documentation of [SciPy](#), the library on which we rely for the computation of the Voronoi diagrams. This choice is intended to facilitate the understanding of the code.

2. Build the Point Voronoi Diagram using  $\bigcup_{c_i \in C} P_{c_i}$  as generators.

3. Delete the Voronoi ridges generated from points that belong to the same component.

Note that, while the Voronoi regions in the Area Voronoi Diagram associated with points in  $\mathbb{R}^2$  need not be polygons, those arising from this approximation shall be. Indeed, in this approximated version, each ridge is a *polygonal chain* made up of Voronoi ridges that separate the same two connected components.

In the following sections, we will refer to *Voronoi diagrams* as the collection of Voronoi ridges that define the boundaries of the Voronoi regions, rather than as the sets of Voronoi regions themselves as defined in Equation (2) or Equation (4). Note that these two are equivalent.

### 3 Method

The method proposed by Kise et al. [8] builds on the approximated Area Voronoi Diagram, described in Section 2.3, using the connected components of the document image as generators. The authors state that the ridges obtained using such a construction represent the candidates for the boundaries of the document *parts*<sup>3</sup>. In this setting, page segmentation translates to selecting those Voronoi ridges that are actually associated with those boundaries.

Equivalently, this problem can be stated as the deletion of superfluous ridges that lie between elements in the same document part. To do so, the method relies on two characteristic features of these ridges: i) the connected components separated by them are *close* and ii) their areas are *similar*. The result of the above deletion process or *pruning* usually destroys the structure of the Area Voronoi Diagram, leaving many isolated ridges and ridges that do not define closed boundaries. Therefore, a final pruning step is applied in order to keep only those meaningful ridges that actually define regions.

The following sections describe the algorithm as proposed by the authors. We highlight the details that are left undefined or that are ambiguous in the original article and explicitly describe how we handle these points in our implementation. A concise summary of the method pipeline is given in Figure 2.

#### 3.1 Binarization

The method [8] takes as input a binary image  $I$  whose connected components are assumed to be the relevant objects for document segmentation, such as characters, symbols and graphics. It is not specified how to deal with non-binary inputs, such as grayscale or RGB images.

Our implementation provides a preprocessing step to binarize such images. If the input is a color image, we obtain a grayscale image  $I_G$  by averaging the color channels. Then,  $I_G$  is thresholded to obtain a binary image. In our implementation, the threshold used at this step can be set manually to an arbitrary value or it can be computed automatically using Otsu's thresholding method [10].

We describe this method here for completeness. Let  $g$  be the empirical distribution of the pixels in the grayscale input  $I_G$  which range between 0 and  $M - 1$ ;  $g_i$  being the value for the  $i$ -th grayscale level. Otsu's threshold  $\tau$  is the value that minimizes the intra-class variance of the two classes of pixel intensities

$$\tau = \arg \min_t \left\{ \sum_{i \leq \tau} g_i (i - \mu_0)^2 + \sum_{j > \tau} g_j (j - \mu_1)^2 \right\}, \text{ where } \mu_0 = \sum_{i \leq \tau} g_i i \text{ and } \mu_1 = \sum_{j > \tau} g_j j. \quad (5)$$

<sup>3</sup>The original paper refers to these as document *components*, but this is quite confusing as components are also referred to as the connected components of the image. Instead, we shall refer to them as document *parts* hereafter.

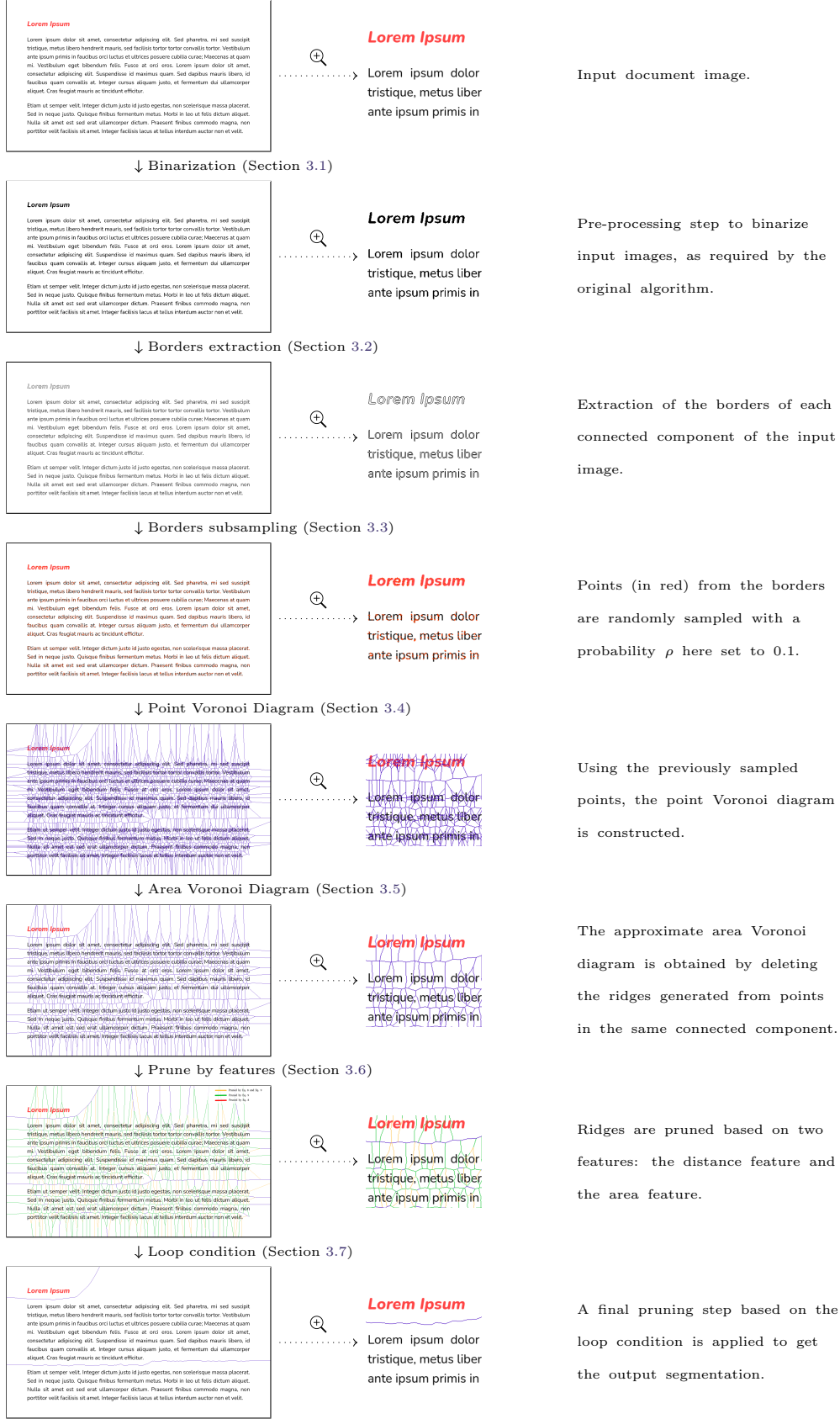


Figure 2: Summary of the main steps of the method's pipeline together with their intermediate outputs.

Assigning a different value to each of these two classes gives the desired binary output.

### 3.2 Labeling of Connected Components and Extraction of Border Points

For digital images, which are defined over a finite, discrete grid of coordinates  $\Omega \subset \mathbb{N}^2$ , the set of components  $C$  described in Section 2.2 can be fully specified by a *labeling map*: this is a pseudo-image where a positive value  $1 \leq r = C(i, j) \leq n$  indicates that the point at  $(i, j) \in \Omega$  belongs to the component  $c_r \in C$ , and  $C(i, j) = 0$  indicates that the corresponding point  $(i, j)$  does not belong to a connected component. Using this map, a connected component  $c_r$  can be recovered from the label map as  $c_r = \{(i, j) \in \Omega : C(i, j) = r\}$ . As both definitions of  $C$  equivalent, we will use the *label map* formalism hereafter.

For digital images, there is no unique definition of connectivity: the most common alternatives are 4-connectivity and 8-connectivity. In the former case, two pixels are considered connected only if they are either one above the other, or one next to the other. In the latter case, they are also considered connected if they are adjacent in any diagonal direction.

The original work [8] uses a *border following* method [7] which produces an 8-connectivity label map and gives the borders of the connected regions as a byproduct. While the implementation of such a method is necessary to guarantee full reproducibility of the original method, it is outside the scope of this paper, as it would imply the complete reproduction of another algorithm. Furthermore, it is not a core part of the algorithm. Therefore, we opt to rely on off-the-shelf solutions: connected components are extracted from the binary image using the `morphology` module in `scikit-image`, and borders are obtained by eroding the binary image and subtracting the result from the original. More details on the implementation are given in Section 5.

A simple denoising strategy is also applied at this point: small connected components having borders of length smaller than  $N$  pixels are discarded. According to Kise et al. [8], the value of  $N$  depends on the resolution of the document image. In their experiments, they vary this value between 4 and 13, without giving specific criteria for setting this parameter. The result of this step is the set of all border points, which we shall refer to as  $B$ .

### 3.3 Borders Subsampling

As stated in Section 2.3, the Point Voronoi Diagram is constructed from a subset  $P$  of the border points in  $B$ . As mentioned in Section 3.2, the original paper [8] uses a border tracking method to extract border points. Based on this, they use this border parametrization to keep every  $R$ th pixel, with  $R$  being a parameter of the method.

Our choice is an independent random sampling where a border point from  $B$  is kept in  $P$  with probability  $\rho$  and discarded otherwise. In principle, all the points can be used: this approach would yield the *exact* Area Voronoi Diagram and, according to our experiments, often better results. However, the computational cost of doing so might be too high. This parameter is actually important, as it defines a quality/computational cost trade-off. The value of this parameter has a non-negligible effect on the final result, which we shall explore in Section 6.

### 3.4 Point Voronoi Diagram

In this step, we construct the Point Voronoi Diagram  $\mathcal{V}(P)$  using the set of sampled border points  $P$  as input, as described in Section 2.1. Two sampled border points (the generators) are associated with each ridge. These are the two input points that are closest to the ridge and equidistant from it by definition. Depending on whether the ridge is finite, half-finite or infinite it will also have two, one or zero vertices associated with it. These vertices are important for later stages of the algorithm.

### 3.5 Approximate Area Voronoi Diagram

The next step is to obtain the approximate Area Voronoi Diagram  $\mathcal{V}(C)$  from the Point Voronoi Diagram, as described in Section 2.3. This is done by removing the ridges in  $\mathcal{V}(P)$  generated by points from the same connected component. In the resulting diagram, the elements are no longer lines or segments but polygonal chains. This is an important difference compared with the original Point Voronoi Diagram. Note that, given the discrete nature of images, this would still be true even if we compute the exact Area Voronoi Diagram. However, this is no longer the case for the Area Voronoi Diagram of a set of connected components in  $\mathbb{R}^2$ , where ridges may include smooth curves.

### 3.6 Pruning by Features

All ridges in the resulting Area Voronoi Diagram lie between two neighboring connected components. As document parts are sets of connected components, the set of Voronoi ridges contains the actual boundaries of the different parts. Here we shall introduce two features used by the authors to decide if a ridge is superfluous or not: the distance between the connected components separated by it, and the ratio between their areas.

Given a ridge  $r = \{l_1, \dots, l_n\}$ , there exist two connected components  $c_i$  and  $c_j$  separated by it. By construction, each line segment  $l_k$  in  $r$  is generated by a pair of points  $p_i^k$  and  $p_j^k$  lying on the boundary of  $c_i$  and  $c_j$  respectively. The *distance feature* associated with the ridge  $r$  is defined as [8]

$$D(r) = \min_{k=1, \dots, n} d(p_i^k, p_j^k). \quad (6)$$

Gaps between characters, words and text lines are narrower than those separating paragraphs or columns. However, relying solely on the distance feature in order to discard superfluous ridges may induce errors. Indeed, there are some cases where ridges separating different document parts are not associated with a large value of  $D$ . This is where the area of the connected components comes into play, as different document parts that lie close to each other usually have different areas.

This observation is captured by the area feature. Consider again a ridge  $r$  and the two connected components  $c_i$  and  $c_j$  separated by it. The *area feature* associated with the ridge  $r$  is defined as [8]

$$A(r) = \frac{\max\{a(c_i), a(c_j)\}}{\min\{a(c_i), a(c_j)\}}. \quad (7)$$

This pruning step aims at discarding ridges based on the above described features. A Voronoi ridge  $r$  is deleted if it satisfies one of the following conditions

$$D(r) < T_1, \quad \text{or} \quad (8)$$

$$\frac{D(r)}{T_2} + \frac{A(r)}{T_A} < 1, \quad (9)$$

where  $T_1$  and  $T_2$  are distance thresholds satisfying  $T_1 < T_2$  and  $T_A$  is an area threshold. The intuition behind these criteria is that very close connected components, such as characters in the same word, are part of the same document part (Equation (8)). Additionally, not-so-close connected components that have similar areas, such as characters in different words or lines, are also part of the same document part (Equation (9)).

These criteria require setting values for the thresholds. The area threshold  $T_A$  is fixed by the authors to 40 as they argue that this value approximately corresponds to the largest area ratio between characters of the same font and size. On the other hand, the distance thresholds  $T_1$  and  $T_2$  are estimated from the image itself. To do so, the method relies on the histogram  $h$  of ridge distance

features, discretized with step 1 and smoothed using an average filter over a symmetric window of size  $2 \times w + 1$ , where  $w$  is an integer parameter. An example of such a histogram is given in Figure 3, together with its corresponding smoothed version when setting  $w = 2$ . According to the paper [8], the value of  $w$  depends on the resolution of the document image. In their experiments, they vary this value between 0 and 2, without giving a specific criterion on how to set this parameter.

This histogram typically has three peaks indicating the most common spacing types: one for distances between letters, another one for the distance between words and another for distances between lines. According to the authors, the two largest ones,  $h_{v_1}$  and  $h_{v_2}$ , with  $v_1 < v_2$  correspond to the inter-character distance and to the inter-line distance, respectively. Indeed, the peak for word spacing is generally smaller because fewer characters are located at the edges of words compared to the number between lines or within words.

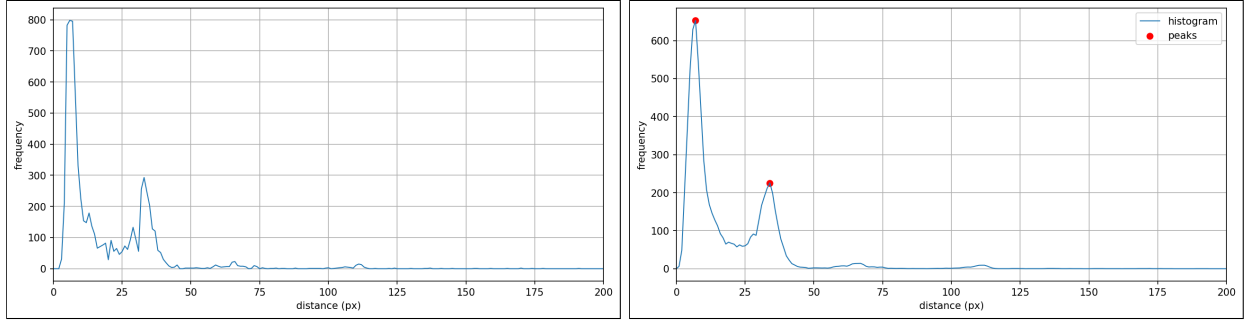


Figure 3: Raw distance features histogram (left) and its smoothed version (right) corresponding to the input document in Figure 2. The smoothed version is obtained using an average filter over a symmetric window of size 5. In red, the largest peaks found in the smoothed histogram.

As the distance between document parts is usually bigger than the inter-character distance, the authors set  $T_1$  to  $v_1$ . However,  $v_2$  is not an appropriate value for  $T_2$  as it only captures the maxima and not the whole mode. Indeed, inter-line distances will concentrate around this value but might exhibit bigger values. To tackle this issue, the authors add a margin to  $v_2$  and define  $T_2$  as

$$T_2 = \min T \quad \text{such that} \quad \begin{cases} T > v_2 \\ h_T = th_{v_2} \end{cases} \quad (10)$$

where  $t$  is the *margin parameter*, set to 0.34 by the authors. As the histogram takes on discrete values, the optimum value of  $T_2$  satisfying Equation (10) is found using linear interpolation.

### 3.7 Loop Condition

The diagram obtained once ridges are deleted based on their distance and area features needs further processing. Indeed, some Voronoi ridges that survive the previously described pruning procedure may not be part of the boundaries of a closed region. In order to discard those ridges, the authors define the *loop condition*: a ridge is said to satisfy the said condition if each of its vertices is either shared by another ridge or lies on the edge of the page. Ridges not satisfying the loop condition are irrelevant for delimiting of document parts. Therefore, the final step of the method consists of discarding them.

## 4 Demo

In this section, we provide a brief explanation of how to use the online demo.

**Input.** The demo expects a single image as input, which may be binary, grayscale, or color. The most common image formats are accepted, but as soon as the image is uploaded, the system will convert it to an 8-bit-per-channel image. The maximum size allowed by the system is  $3000 \times 3000$  pixels. If the input is larger than this, the demo will still work, but it will resize the image to meet the size requirement. In this case, the demo displays a warning message:

Input #0 has been preprocessed {resized X%},

where  $X$  stands for the resizing factor needed to fulfill the size requirement.

It is important to mention that these restrictions are needed by the system to guarantee a reasonable runtime but are not part of the source code. To avoid those, we advise the interested users to download and run the provided code locally.

**Parameters.** By default, the demo shows five parameters:

- Binarization mode: Defines the binarization method used for non-binary input images, as described in Section 3.1. The options are *Otsu's thresholding* and *Custom thresholding*. If the user selects the custom option, a threshold parameter is displayed for the user to choose a value in the range 1-255.
- $N$ : Defines the denoising strategy to be applied, according to Section 3.2. If set to zero, no denoising is applied. If set to a value larger than zero, this will remove all blobs whose sizes are smaller than the specified value. The original method [8] does not specify a value for this parameter but, in their experiments, they vary it between 4 and 13. The user may choose a value between 0 (no denoising) and 13, with 4 being the default one.
- $\rho$ : Defines the borders subsampling parameter, as described in Section 3.3. By setting this parameter, the user establishes the probability that a border point is kept. This parameter is actually important, as it defines a quality/computational cost trade-off. This parameter ranges from 0.01 to 1, with 0.1 as the default value.
- $w$ : Defines a window of size  $2 \times w + 1$  over which the histogram of distances between connected components is smoothed by averaging during the pruning step (see Section 3.6). The paper [8] does not clearly state a criterion for whether to smooth the distance features histogram. Furthermore, the size of the smoothing window is not clearly defined. We allow the user to set this parameter between 0 (no smoothing) and 4, with 2 as the default value.
- $T_A$ : Defines the area threshold in the pruning criteria defined by Equation (9) during the pruning by features step (Section 3.6). The original method sets it to 40, arguing that this value approximately corresponds to the largest area ratio between characters of the same font and size. The demo allows the user to set this parameter to any value between 10 and 70, allowing users to test other values that may be better suited to their use case.

**Outputs.** The outputs are displayed as a gallery of PNG images. The images shown in this gallery follow the method's pipeline, as in Figure 2. These are:

- Input: Input image, as submitted by the user.
- Binary input: Binary image obtained after the binarization step (Section 3.1).
- Blobs removed: Resulting image after small blobs (defined by parameter  $N$ ) are removed. If  $N$  is set to 0, this image is the same as the previous one.

- Extracted borders: Image displaying the borders of the connected components extracted by the method according to Section 3.2.
- Borders samples: Image displaying in red, on top of the borders, the points that have been sampled to construct the Voronoi Diagram (see Section 3.3). For visualization purposes, sampled points are slightly thickened.
- Point Voronoi Diagram: Point Voronoi Diagram computed using the sampled border points as generators (see Section 3.4).
- Area Voronoi Diagram: Area Voronoi Diagram obtained once redundant ridges are pruned (see Section 3.5).
- Distances histogram: Histogram of the ridge distance features (Equation (6)), discretized with step 1, as described in Section 3.6.
- Smoothed distances histogram: Histogram after smoothing using an average filter over a symmetric window of size  $2 \times w + 1$ . Note that here  $w$  takes the value chosen by the user. If it is 0, the original histogram will be displayed. The peaks found by the method are painted in red.
- Pruned by features: Diagram obtained once the Area Voronoi Diagram is pruned by the distance and area features, according to Equation (8) and Equation (9). The pruned ridges are painted in different colors according to the criterion that removed them: red for Equation (8), green for Equation (9) and orange for both.
- Final segmentation: Final diagram once the loop condition is imposed, as described in Section 3.7. This is the actual output of the method.

**Log file.** Besides the visual results displayed in the gallery, the method also outputs a log file which provides the user with information about the execution. For a standard execution, these messages include the number of connected components found in the image, the border points and how many are sampled, the number of ridges and vertices of both the Point Voronoi Diagram and the Area Voronoi Diagram, the numerical value of the peaks found in the histogram and the distance thresholds computed from them, the number of pruned ridges and the criterion used to prune them, finally, the number of ridges in the final diagram. Warning messages can also be displayed in the log file. These indicate potential issues or risks that occurred during the execution but did not stop the program from running. In those cases, we advise the user to check for unintended behavior.

However, if there were errors during the execution, not all of this information shall be provided. In that case, the log file will show a message explaining the type of error encountered. Some common errors include having only a single connected component in the image, missing border points, insufficient points to construct the Point Voronoi Diagram, or the absence of peaks in the distances histogram.

## 5 Detailed Implementation

The whole algorithm is implemented in a single executable Python file `voronoi.py`; a few utilities are provided separately in `util.py`. The program provides a command-line where the user can optionally modify the default parameters of all stages and choose alternatives for those parts that are not completely specified.

---

**Algorithm 1:** Voronoi document layout analysis algorithm.

---

**Input**  $I$ : binary image.  
**Output**  $\mathcal{V}^*$ : resulting segmentation diagram.

---

```

1  $C \leftarrow \text{get\_connected\_components}(I, N)$ 
2  $B \leftarrow \text{get\_borders}(C)$ 
3  $P \leftarrow \text{sample\_border\_points}(B, \rho)$ 
4  $\mathcal{V}(P) \leftarrow \text{get\_point\_voronoi}(P)$ 
5  $R \leftarrow \text{eval\_redundancy\_criterion}(\mathcal{V}(P), C)$            # bool. list, one entry per ridge
6  $\mathcal{V}(C) \leftarrow \text{ridges } r_i \text{ in } \mathcal{V}(P) \text{ such that } R_{r_i} = 1$ 
7  $D, A \leftarrow \text{compute\_ridge\_features}(\mathcal{V}(C), C)$ 
8  $T_1, T_2 \leftarrow \text{compute\_thresholds}(D, t, w)$ 
9  $P \leftarrow \text{eval\_pruning\_criteria}(\mathcal{V}(C), D, A, T_1, T_2, T_A)$       # bool. list, one entry per ridge
10  $\bar{\mathcal{V}} \leftarrow \text{ridges } r_i \text{ in } \mathcal{V}(C) \text{ such that } P_{r_i} = 1$ 
11  $\mathcal{V}^* \leftarrow \text{prune\_by\_loop\_condition}(\bar{\mathcal{V}})$ 
12 return  $\mathcal{V}^*$ 

```

---

The complete method, which is described in Algorithm 1, is divided into functions that correspond to each step defined in Section 3. We will now describe each of these using the actual function names for easy cross-reference with the code.

$I = \text{get\_binary\_image}(I_{\text{input}})$  Converts the submitted image  $I_{\text{input}}$  into a binary image  $I$ . This includes removing transparency (alpha channel) if present, converting color images to grayscale, and thresholding the grayscale image in order to obtain a binary representation. Details on the latter are provided in Section 3.1.

$C = \text{get\_connected\_components}(I, N)$  Produces a label map  $C$  where  $C(i, j) = 0$  indicates that the pixel at position  $(i, j)$  in image  $I$  is background and  $C(i, j) = c > 0$  means that the corresponding pixel in  $I$  belongs to a connected component identified by the label  $c$ . Connected components having borders of length smaller than  $N$  pixels are discarded.

$B = \text{get\_borders}(C)$  Returns the bordering pixels of the connected components as a binary image. This is obtained as the difference between the binarized input image and a binary erosion of it using a 4-neighbors kernel.

$P = \text{sample\_border\_points}(B, \rho)$  Samples border points randomly using a  $Z \sim \text{Bernoulli}(\rho)$  process where  $Z = 1$  indicates to keep the point and 0 to discard it.

$\mathcal{V} = \text{get\_point\_voronoi}(P)$  Takes the sampled border points as inputs and produces the initial Point Voronoi Diagram. This is computed using [SciPy](#).

$R = \text{eval\_redundancy\_criterion}(\mathcal{V}(P), C)$  Returns a list of boolean values with a 1 in the  $i$ -th position for those Point Voronoi ridges that should be kept, and 0 otherwise. This is described in Algorithm 2. The approximate Area Voronoi Diagram  $\mathcal{V}(C)$  is obtained once redundant ridges are discarded.

Note that, at this step we **do not** merge the Point Voronoi ridges into Area Voronoi ridges. Ridges are structurally kept as the original line segments. This detail is important in Algorithm 3.

$D, A = \text{compute\_ridge\_features}(\mathcal{V}(C), C)$  Computes the distance  $D(r)$  and area  $A(r)$  ratio features of each ridge  $r$  in  $\mathcal{V}(C)$ . This is explained in Section 3.6. Algorithm 3 provides the pseudocode for this function.

Note that, when computing  $D_r$ , the distances are not the actual distances between the components but the distances between sampled points from their borders.

$T_1, T_2 = \text{compute\_thresholds}(D, t, w)$  Computes the thresholds defined in Section 3.6. The pseudocode is provided in Algorithm 4.

$P = \text{eval\_pruning\_criteria}(\mathcal{V}(C), C, D, A, T_1, T_2, T_A)$  Returns a list of boolean values  $P$  where  $P_i = 0$  indicates that the  $i$ -th ridge,  $r_i$ , does not satisfy Equation (8) and Equation (9) and thus should be removed. The pseudocode for this function is given in Algorithm 5.

$L = \text{eval\_loop\_condition}(\bar{\mathcal{V}})$  Returns a boolean list  $L$  where a 0 in the  $i$ -th element indicates that the corresponding ridge in  $\bar{\mathcal{V}}$  does not satisfy the loop condition. See Algorithm 6.

$\mathcal{V}^* = \text{prune\_by\_loop\_condition}(\bar{\mathcal{V}})$  This function takes  $\bar{\mathcal{V}}$  as input and prunes those elements that do not satisfy the loop condition iteratively until no further pruning occurs, producing  $\mathcal{V}^*$ . This is described in Algorithm 7.

---

**Algorithm 2:** eval\_redundancy\_criterion.

---

**Input**  $\mathcal{V}(P)$ : Point Voronoi Diagram  
**Input**  $C$ : label map  
**Output**  $R$ : pruning indicator vector.  
1 **for** each ridge  $r_k$  in  $\mathcal{V}(P)$  **do**  
2    $p_1, p_2 \leftarrow$  generator points of ridge  $r_k$   
3    $R_k \leftarrow \text{boolean}(C(p_1) \neq C(p_2))$   
4 **return**  $R$

---



---

**Algorithm 3:** compute\_ridge\_features.

---

**Input**  $\mathcal{V}(C)$ : Voronoi ridges (line segments)  
**Input**  $C$ : label map  
**Output**  $D$ : distance features  
**Output**  $A$ : area ratio features  
1  $n \leftarrow \max C$  # number of connected components  
2  $D_{i,j} \leftarrow +\infty$ ,  $i, j = 1, \dots, n$   
3  $A_{i,j} \leftarrow 0$ ,  $i, j = 1, \dots, n$  # initial value does not matter  
4 **for** each line segment  $l$  in  $\mathcal{V}(C)$  **do**  
5    $p_1, p_2 \leftarrow$  generator points of line segment  $l$   
6    $i, j \leftarrow C(p_1), C(p_2)$  # labels of the connected components of  $p_1, p_2$  resp.  
7    $c_i, c_j \leftarrow$  connected components for labels  $i$  and  $j$  in  $C$   
8    $A_{i,j} \leftarrow \frac{\max(|c_i|, |c_j|)}{\min(|c_i|, |c_j|)}$  # computes Equation (7)  
9    $D_{i,j} \leftarrow \min\{D_{i,j}, \|p_1 - p_2\|_2\}$  # iteratively computes Equation (6)  
10 **return**  $D, A$

---

---

**Algorithm 4:** compute\_thresholds.

---

**Input**  $D$ : distance features  
**Param**  $w$ : smoothing window size parameter  
**Param**  $t$ : margin parameter (set to 0.34)  
**Output**  $T_1, T_2$ : thresholds

- 1  $\tilde{h} \leftarrow$  histogram of  $D$
- 2  $h \leftarrow$  smoothed histogram,  $h_i = \frac{1}{2w+1} \sum_{k=-w}^w \tilde{h}_{i+k}$  **# out-of-range values are repeated**  
**# below, if only one peak is found, we set  $v_1 = v_2$**
- 3  $v_1, v_2 \leftarrow$  index of the two largest peaks of  $h$  in ascending order
- 4  $T_1 \leftarrow v_1$
- 5  $T \leftarrow v_2$
- 6 **while**  $h_T > th_{v_2}$  **do**
- 7    $T \leftarrow T + 1$
- 8  $T_2 \leftarrow T - 1 + \frac{th_{v_2} - h_{T-1}}{h_T - h_{T-1}}$  **# computes Equation (10) using linear interpolation**
- 9 **return**  $T_1, T_2$

---



---

**Algorithm 5:** eval\_pruning\_criteria.

---

**Input**  $\mathcal{V}(C)$ : Voronoi ridges (line segments)  
**Input**  $C$ : label map  
**Input**  $D$ : distance features  
**Input**  $A$ : area ratio features  
**Param**  $T_1$ : Threshold 1  
**Param**  $T_2$ : Threshold 2  
**Param**  $T_A$ : area threshold  
**Output**  $P$ : pruning indicator vector (boolean)

- 1 **for** each line segment  $l_k$  in  $\mathcal{V}(C)$  **do**
- 2    $p_1, p_2 \leftarrow$  generator points of line segment  $l_k$
- 3    $i, j \leftarrow C(p_1), C(p_2)$  **# labels of the connected components of  $p_1, p_2$  resp.**
- 4    $c_1 = C(i_1); c_2 = C(i_2)$  **# components with labels  $i$  and  $j$**
- 5    $P_k = D_{i,j} \geq T_1$  and  $D_{i,j}/T_2 + A_{i,j}/T_A \geq 1$  **#  $P_k = 1$  means keep**
- 6 **return**  $P$

---



---

**Algorithm 6:** eval\_loop\_condition.

---

**Input**  $\mathcal{V}(C)$ : Voronoi ridges  
**Output**  $L$ : Pruning indicator vector

- 1 **for** each line segment  $l_k$  in  $\mathcal{V}(C)$  **do**
- 2    $v_1, v_2 \leftarrow$  vertices of  $l_k$   
**# the vertex value  $\infty$  below means border vertex;  $L_k = 1$  means keep**
- 3    $L_k \leftarrow v_1$  not only in  $l_i$  or  $v_1 = \infty$  and  $v_2$  not only in  $l_i$  or  $v_2 = \infty$
- 4 **return**  $L$

---

**Algorithm 7:** prune\_by\_loop\_condition.

---

**Input**  $\bar{\mathcal{V}}$ : Voronoi ridges  
**Output**  $\mathcal{V}^*$ : Pruned ridges

- 1  $\mathcal{V}^* \leftarrow \bar{\mathcal{V}}$
- 2 **repeat**
- 3      $L \leftarrow \text{eval\_loop\_condition}(\mathcal{V}^*)$
- 4      $\mathcal{V}^* = \{r_k \in \mathcal{V}^* : L_k = 1, k = 1, \dots, |\mathcal{V}^*|\}$
- 5 **until**  $L$  is all ones
- 6 **return**  $\mathcal{V}^*$

---

## 6 Experiments

### 6.1 Impact of the Parameters

**Binarization mode.** While Otsu’s thresholding method enables us to automate the binarization procedure by minimizing intra-class intensity variance, custom thresholding might work better in some cases, as shown in Figure 4. In this example, the background is completely white and the foreground exhibits several grayscale intensities. Otsu’s threshold takes parts of the figures as background, causing an over-segmentation of the document that does not respect the figures’ borders. On the other hand, a custom threshold set to a value close to 255 (250 in this example) correctly identifies the pictures in the document as foreground. The final segmentation with this thresholding approach correctly respects figures’ boundaries.



Figure 4: Comparison between Otsu’s thresholding and custom thresholding. When binarization is performed using Otsu’s threshold, parts of the pictures in the document are taken as background, causing an incorrect segmentation of those parts. A custom threshold set to 250 prevents such behavior and outputs correct region borders. The results shown here are obtained by setting  $N = 4$ ,  $w = 2$ ,  $\rho = 0.4$  and  $T_A = 40$ .

**Blobs removal parameter  $N$ .** The parameter  $N$  sets the size of blobs to be discarded as noise. Its optimal value depends, of course, on the noise present in the document as well as on its resolution. Kise et al. [8] vary this parameter across their experiments without setting a clear criterion for its selection. While this parameter can be irrelevant for noiseless documents such as most modern digital documents, it might be crucial to achieve a satisfactory result in noisy ones. Figure 5 shows such an example. If no denoising is applied, the final segmentation presents several document parts that are semantically meaningless to the document layout. This is because each blob is considered a generator for the Area Voronoi Diagram construction. When setting  $N = 2$ , this phenomenon is mitigated, but  $N = 2$  is not enough to successfully remove all the noise. Setting  $N = 3$  indeed produces the desired output: blobs due to noise are correctly removed and the final segmentation actually reflects the document layout. However, there is an undesirable side effect: characters (or part of them) may also be removed. This becomes more evident when setting  $N = 13$ . In this case, entire parts of the text are deleted and this causes an incorrect segmentation of the document parts.

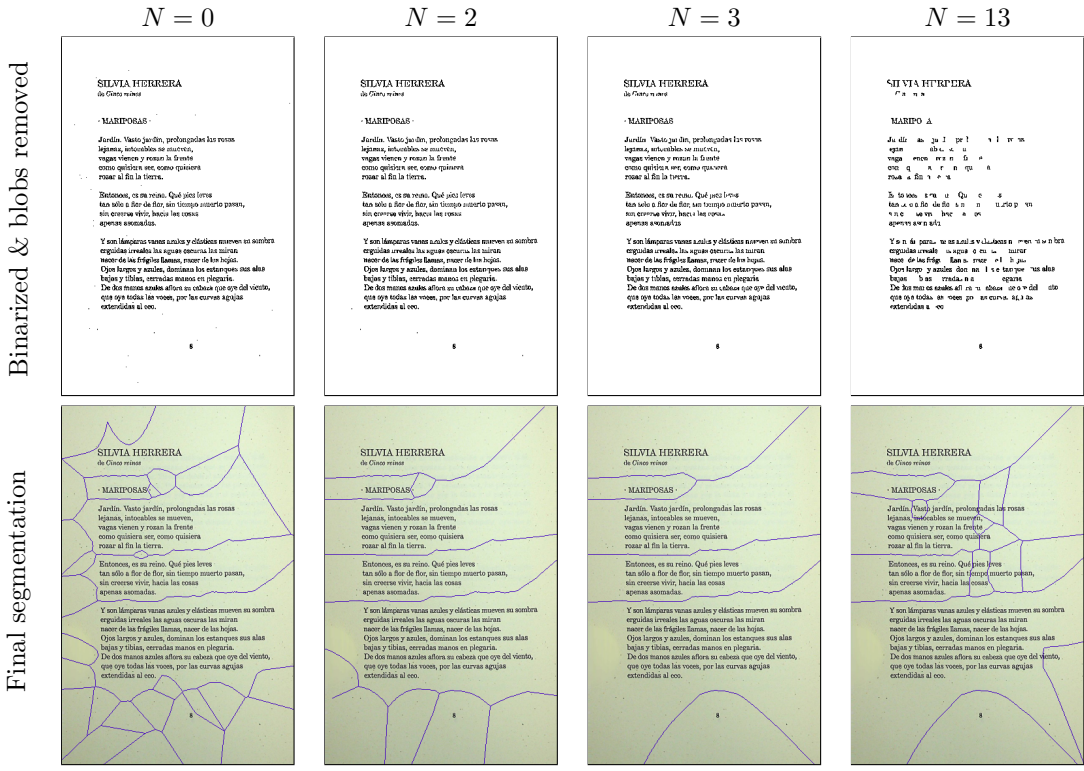


Figure 5: Comparison between different values for the blobs parameter  $N$ . When no denoising is applied ( $N = 0$ ) or when it is insufficient, the final segmentation generates document parts that are meaningless for the document layout. Setting  $N = 3$  produces the correct output. An excessive denoising ( $N = 13$ ) can produce the loss of parts of the text and artifacts in the final segmentation. The results shown here can be replicated by setting *Otsu's thresholding* as binarization mode,  $w = 2$ ,  $\rho = 1$  and  $T_A = 40$ .

While tuning the parameter  $N$  can be effective in many cases, there exist degraded documents for which no value yields a satisfactory result. Figure 6 illustrates such an edge case, where the document suffers from two simultaneous issues: the presence of large blobs of noise, and the fragmentation of characters due to insufficient ink or fading. In this scenario, setting  $N$  too low results in the inclusion of noisy regions as valid layout elements, while increasing  $N$  inevitably removes legitimate text components that appear small due to degradation. As a consequence, segmentation either fails to discard noisy areas or disrupts the structure of textual elements. This example highlights the limitations of blob-size filtering alone and suggests that more robust noise handling strategies may be necessary for highly degraded documents.

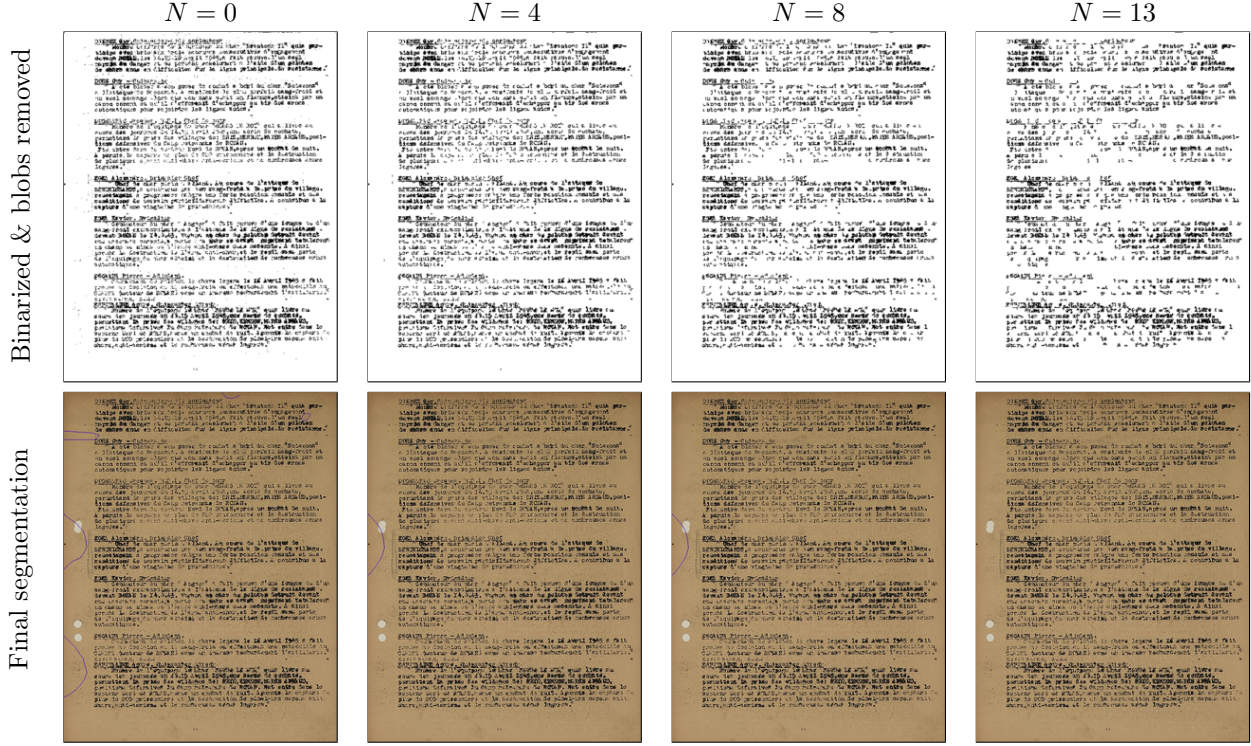


Figure 6: Limitations of blob-size filtering in a severely degraded document. The input document contains both large blobs of noise and fragmented characters due to ink loss. Varying the parameter  $N$  demonstrates the trade-off: small values fail to remove noisy regions, while larger values eliminate valid character fragments. No value of  $N$  yields a clean segmentation, illustrating the need for more sophisticated denoising strategies in such cases. The results shown here can be replicated by setting *Otsu's thresholding* as binarization mode,  $w = 2$ ,  $\rho = 0.1$  and  $T_A = 40$ .

**Smoothing window size  $w$ .** A key element in the success of the method [8] is the determination of the thresholds  $T_1$  and  $T_2$ , which are derived from the two largest peaks in the histogram of distances between the components, as described in Section 3.6. The rationale behind the determination of  $T_1$  and  $T_2$  from the two largest peaks is that these peaks correspond to the centers of the two main modes typically observed in these histograms: one for distances between letters, and another for distances between lines.

However, the distance between two components, be it within a word or between different lines, is actually a noisy estimator of the inter-character or inter-line distances. Indeed, as characters have different shapes, this distance is affected by the particular characters involved in the measurement. Features like tall letters (ascenders), letters that go below the line (descenders), and capital letters especially affect the measurement of line spacing. Additionally, the distance between two components is measured using the generator points rather than the component itself. Therefore, the subsampling parameter  $\rho$  also adds noise to the histogram.

To reduce this noise and make the estimates clearer, the original method proposes smoothing the histogram using an average filter over a symmetric window of size  $2 \times w + 1$ . The size of this window, given by  $w$ , is left as a parameter of the method. In Figure 7 we illustrate the effect of this smoothing. When no smoothing is applied ( $w = 0$ ), the two highest peaks are very close and seem to be part of the same noisy mode. Presumably, both represent the inter-character distance as, in the final segmentation, words are separated into different cells. On the other hand, when smoothing is applied ( $w = 2$  or  $w = 4$ ), these two peaks are merged into one and the second highest peak in this case seems to accurately correspond to the inter-line distance. The final segmentation seems to corroborate this, as paragraphs are correctly identified as belonging to the same region. It is worth mentioning that the main difference between setting  $w = 2$  and  $w = 4$  is that while the peaks are



Figure 7: Effect of the smoothing window size  $w$  on the distances histogram, the pruning by features step, and the final segmentation. When no smoothing is applied ( $w = 0$ ), the two largest peaks seem to correspond to the same noisy mode, resulting in an erroneous segmentation. On the other hand, when smoothing is applied, these two peaks are merged into one and the second highest peak in this case seems to correspond to the inter-line distance. In this case, the final segmentation accurately represents the document layout. The results shown here can be replicated by setting the binarization threshold to 200,  $N = 4$ ,  $\rho = 0.3$  and  $T_A = 40$ .

still visible with both window sizes, their distance, relative heights, and sharpness change. Larger values of  $w$  shall result in the merging of these two modes.

**Subsampling parameter  $\rho$ .** Subsampling was introduced in the original paper [8] in order to reduce the computation time involved in computing the *exact* Area Voronoi Diagram. Our implementation keeps a random fraction  $\rho$  of the border pixels, which is set by default to  $\rho = 0.1$ . The maximum value  $\rho = 1$  keeps all border pixels, resulting in the exact Area Voronoi Diagram.

As shown in Figure 8, and confirmed in many experiments, for moderate to high resolution images (e.g., above 150 DPI) the approximation obtained with the default value does not introduce artifacts or errors in the resulting segmentation and reduces computational time. On the other hand, for low resolution images (say, below 150 DPI), the default value may result in all border points of an entire component being skipped (in the example, the letter “t”), often degrading the resulting segmentation. At the same time, with modern computational resources, small images are quick to process even with the maximum value  $\rho = 1$ . Therefore, our recommendation is to use  $\rho = 0.1$  unless the input image is small, in which case a larger value is recommended.

Final segmentation

Sampling

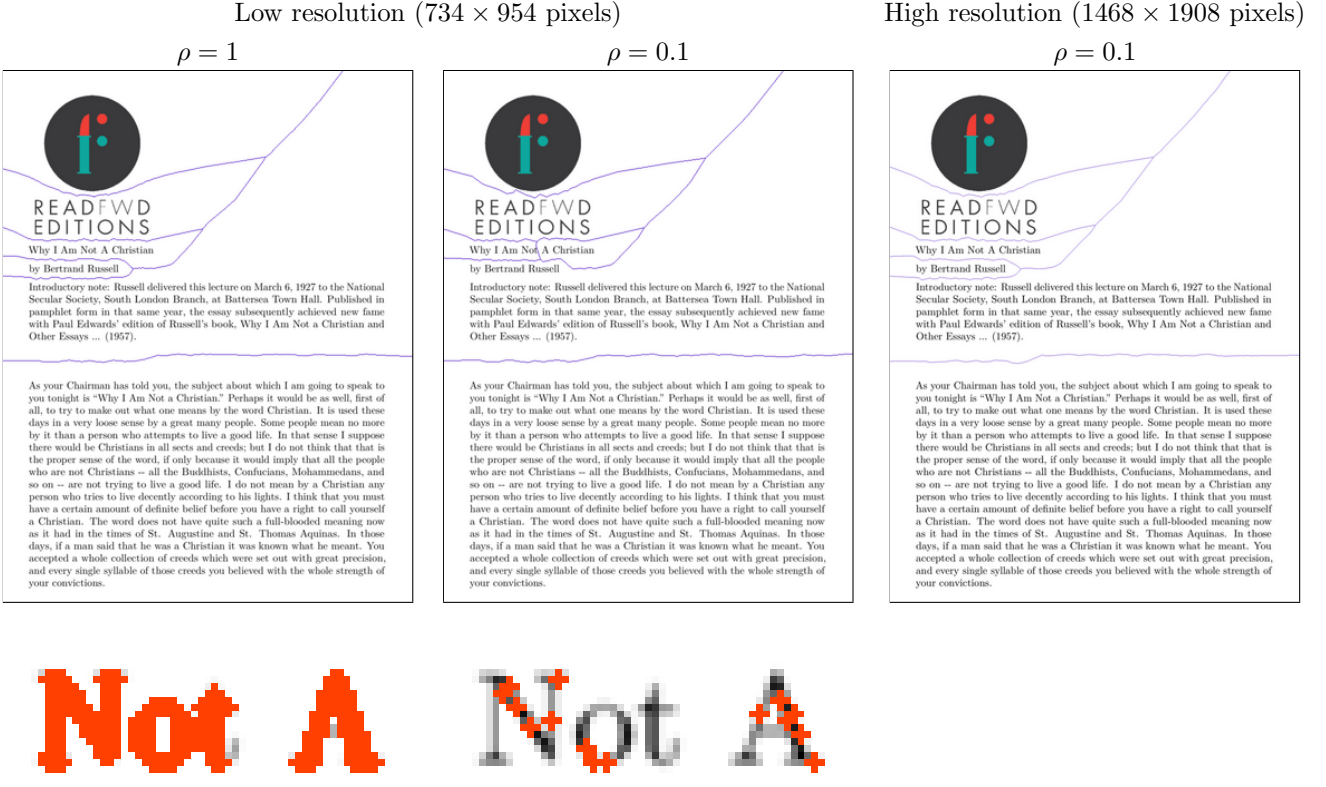


Figure 8: Effect of subsampling parameter  $\rho$ . The first row shows the results obtained on the same page for different resolutions and values of  $\rho$ . From left to right: low resolution with  $\rho = 1$ , low resolution with  $\rho = 0.1$  and high resolution with  $\rho = 0.1$ . There is an error in the segmentation in the second case (middle image), with the title of the book “Why I Am Not A Christian” divided between “Not” and “A”. In the second row we show a zoom of that case where the source of the error can be clearly attributed to the subsampling process: as the letter “t” was completely skipped, the space between the “o” and the “A” surpasses the threshold and therefore it was considered a significant edge. This does not happen when using the full border, as shown on the bottom right image.

**Area threshold  $T_A$ .** The area threshold has a significant role in Equation (9). Still, setting it is not straightforward: it should be permissive enough not to segment characters from the same font and size, even when their areas differ substantially, while still being discriminative enough to distinguish slight differences in the font size. Kise et al. fixed this threshold to 40 once and for all. In our implementation, we allow users to modify this value according to their particular needs. In Figure 9 we show an example of how modifying this threshold can impact the output of the method. Indeed, when setting  $T_A$  to 40, the subtitle “Takeoff and Climb” is not segmented separately from the body text because it lies close to the text and the font size is not significantly larger. Lowering the threshold to 30 results in a better segmentation as the method is better able to discriminate characters having different font sizes.

## 6.2 Analysis of Sample Cases

In this section, we present a series of examples obtained using the analyzed method to illustrate its performance in various scenarios. In each case, we aim to provide a comprehensive understanding of the method’s performance and its strengths and weaknesses. All the examples shown here can be replicated by setting *Otsu’s thresholding* as binarization mode,  $N = 4$ ,  $w = 2$  and  $\rho = 1$ .

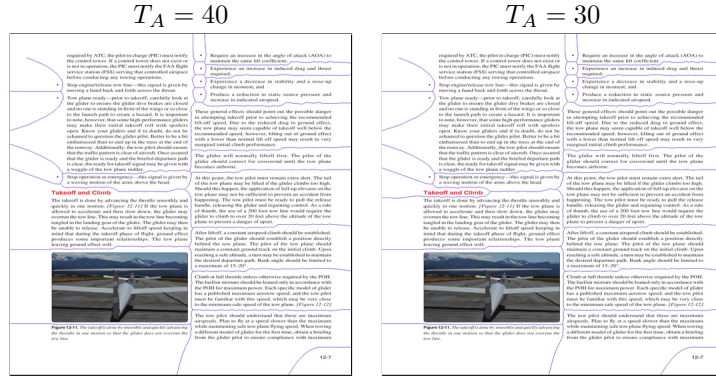


Figure 9: Comparison between different area thresholds ( $T_A$ ). When setting  $T_A$  to 40, as done in the original article, the subtitle “Takeoff and Climb” is not segmented separately as it lies close to the text and the font size is not significantly larger. Setting an area threshold of 30 produces the correct segmentation, as the method becomes more discriminative. The results shown here can be replicated by setting *Otsu’s thresholding* as binarization mode,  $N = 4$ ,  $w = 2$  and  $\rho = 1$ .

**Simple layouts.** Basic layout structures should represent the least challenging scenario for the method. Still, even in these cases, some mistakes can happen. Figure 10 shows the segmentation obtained for three examples. We observe that the method is able to correctly handle multiple columns, as in the first and second document. Still, it is worth mentioning that, when paragraphs are determined by indentation (first document), the method is not able to segment them. On the other hand, when spacing between paragraphs is used (second document), paragraphs are segmented separately. The second document contains a list where inter-line spacing is bigger than in the rest of the document. Note that the method is not consistent in handling such a structure, as some lines are merged together while others are not. This depends on the spacing between ascenders and descenders in each line. Finally, the third example depicts a limitation of the method: text having bigger inter-word spacing than the predominant spacing is likely to be over-segmented.



Figure 10: Results on simple layouts. The method is able to correctly handle multi-column text as well as paragraph separation through spacing. However, document parts with different inter-line or inter-word spacing than in the main text can cause errors in the segmentation.

**Tables.** Tables are versatile layout elements widely used in documents. Naturally, their design can vary depending on the purpose and style of the document: the use of grid-lines, alignment and spacing shall be different in each case. Figure 11 depicts the segmentation obtained in two examples. Simple tables, such as the one in the first document, are correctly handled by the method as multi-column text. However, complex tables, such as the one in the second example, are poorly handled. In this case, grid-lines spanning over multiple columns cause text in different columns to be merged.

into a single cell. On the other hand, extra spacing in the table causes over-segmentation within a single column.

**Radian Group Inc. Notes to Consolidated Financial Statements - (Continued)**

Revolving and direct rates in 2011 and 2012 have been affected by an increase in the number of claims received that we are reviewing for potential recovery. The rates in 2011 and 2012 have been affected by an increase in the number of claims received and reinsurance rates in our total fine-line portfolio, net of both actual and expected reinsurance, as of December 31, 2012, and respectively.

**Claims Received**

Claims Received	Percentage of Claims Received for Loss Reserve (1)	Percentage of Claims Received for Loss Reserve (2)
Q1 2012	18.5%	100%
Q2 2012	18.5%	100%
Q3 2010	16.0%	100%
Q4 2010	17.5%	100%
Q1 2011	20.8%	99%
Q2 2011	23.6%	99%
Q3 2011	28.1%	97%
Q4 2011	23.2%	98%
Q1 2012	21.3%	98%
Q2 2012	20.5%	98%

**Notes**

(1) Projected net cumulative loss/residual rates represent the ratio of claims received or denied to claims received by remaining claims. Revisions and denials are net of actual reinsurance, plus our current estimate for expected reinsurance. Actual reinsurance is the amount of reinsurance received during the period. The projected net cumulative loss/residual rates for the first and second quarters of 2012 have been revised due to the fact that the periods above have been partially resolved. The remaining periods will be revised as more claims are received and reinsurance is received. (2) Based on the projected net cumulative loss/residual rates for each quarter, we have calculated the number of claims that have been internally resolved as a percentage of the total number of claims received for that specific quarter. A claim is considered internally resolved when it is received and the amount of reinsurance received is known. The projected net cumulative loss/residual rates will be challenged and potentially revised as experience, respectively. For the third and fourth quarters of 2012, a significant percentage of the claims received during these periods are possibly straightforward and, therefore, they are not presented as internally resolved.

**Loss Reserves**

For purposes of example, if there were a 10% change in the number of claims received for the third quarter of 2012, we estimated that our loss reserves would change by approximately \$67 million at December 31, 2012. For every additional 10% increase in the number of claims received for the third quarter of 2012, we estimated that our loss reserves would change by approximately \$33 million at December 31, 2012. For every additional 10% decrease in the number of claims received for the third quarter of 2012, we estimated that our loss reserves would change by approximately \$37 million at December 31, 2012. For every additional 10% increase in the number of claims received for the fourth quarter of 2012, we estimated that our loss reserves would change by approximately \$5 million at December 31, 2012. For every additional 10% decrease in the number of claims received for the fourth quarter of 2012, we estimated that our loss reserves would change by approximately \$5 million at December 31, 2012.

**Financial Review 2004**

**Consolidated Statements of Cash Flows**

May 29, 2005	May 26, 2004
\$ 32,042	\$ 24,018
Cash flows - operating activities	
Net cash provided by operating activities	\$ 16,218
Dividends paid	(10,756)
Acquisitions to reconcile net earnings to cash flows:	
Dividends received	48,756
Asset impairment charges, net	(1,513)
Amortization of unearned compensation and loan costs	5,009
Change in fair value of derivatives	2,047
Change in other liabilities	420
Change in cash surrender value of trust-owned life insurance	(1,053)
Change in cash surrender value of life insurance	16,508
Income tax benefit related to equity	942
Interest paid	16,386
Interest received	16,386
Other, net	494
Net cash provided by operating activities	\$ 252
(\$ 32,042)	\$ 30,870
Cash flows - investing activities	
Proceeds from sale of investment stock	(104,320)
Dividends paid	(5,130)
Proceeds from sale of property, plant and equipment	16,000
Proceeds from sale of investments	1,000
Proceeds from maturities of purchases off-shore term investments	1,000
Net cash used in investing activities	\$ (100,350)
(\$ 32,042)	\$ (100,350)
Cash flows - financing activities	
Proceeds from issuance of long-term debt	\$ 116,090
Proceeds from issuance of common stock	\$ 81,948
Dividends paid	(48,650)
Change in cash and cash equivalents, beginning of year	\$ 152,870
Net cash used in financing activities	\$ 145,370
\$ 32,042	\$ 145,370
Cash flows from changes in current assets and liabilities	
Investments	(128,137)
Prepaid expenses and other current assets	(1,300)
Accounts payable	11,077
Accrued liabilities	13,023
Accrued income taxes	(19,223)
Other current assets	2,411
Other current liabilities	2,411
Other non-current assets	24,524
Other non-current liabilities	(1,826)
Change in current assets and liabilities	\$ 2,207
\$ 32,042	\$ 26,054

*See accompanying notes to consolidated financial statements.*

Figure 11: Results on documents containing tables. Simple tables are correctly handled as multi-column text. More complex ones generate an inconsistent segmentation: text in different columns is merged into a single cell while text in the same column is sometimes segmented.

**Light characters on dark backgrounds.** The binarization step in the current implementation assumes that background pixels are lighter than foreground ones. Therefore, whenever text is written in lighter colors than the background, the segmentation shall be unsatisfactory. This situation is depicted in Figure 12. In the first example, simply inverting the colors would be enough to avoid this problem. However, the other two examples would require a local approach, as in those cases dark and light fonts as well as background colors are intermixed throughout the document. We advise users to handle these situations before submitting the image to the demo.



Figure 12: Results on documents with dark backgrounds and light-colored text. The binarization step in the current implementation assumes that background pixels are lighter than foreground ones. Therefore, the segmentation results in these examples are unsatisfactory.

**Drop-caps.** Drop-caps are large, decorative capital letters used at the beginning of a section or paragraph in a document. In terms of semantics, drop-caps are part of the said section or paragraph. However, their style does not match the rest of the body-text. Handling drop-caps is ambiguous and defining whether they should be segmented separately or not depends on downstream applications. Figure 13 presents the segmentation obtained for two examples having drop-caps. We observe that the method is not consistent in its handling of these elements and that the final segmentation depends

on each case. If drop-caps lie very close to the text and their area falls within the limits imposed by Equation (9), they are likely to be merged with the text body, as in the first example. On the other hand, when these criteria are not met, either because they are too large or lie too far from the text (or a combination of both), drop-caps are segmented apart, as in the second example.

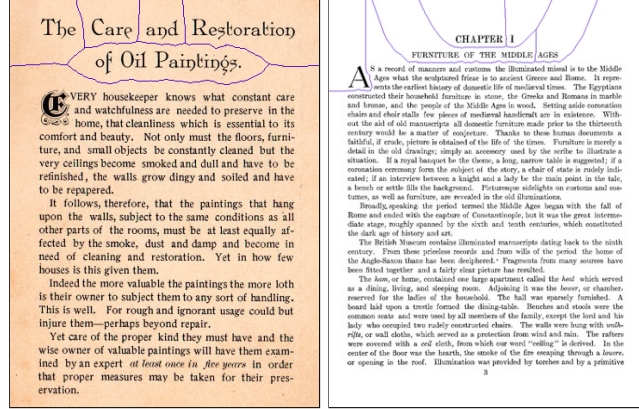


Figure 13: Results on documents with drop-caps. The segmentation depends on each particular case, mostly on the distance between the drop-cap and the main text as well as the relative area with respect to the neighboring characters.

**Non-Manhattan layouts.** Contrary to most of the document layout analysis techniques in the literature [9, 3, 2, 5, 14, 15], handling non-Manhattan layouts involving irregular boundaries is one of the main strengths of the method. Figure 14 illustrates the method’s ability to segment such layouts. In both examples, the irregular boundaries of the text surrounding the figures are correctly managed. Still, note that in the second example, there is an over-segmentation of the figure in the top-right of the document due to binarization artifacts.



Figure 14: Results on non-Manhattan documents. In both examples, the irregular boundaries of the text surrounding the figures are correctly managed.

**Overlapping layouts.** The method is not designed to work on documents where overlapping elements are present. This is, indeed, the most challenging scenario for document layout analysis. When analyzing such documents, two situations can be encountered. First, the overlapping elements can be taken as part of the background when binarizing the document; consequently, the resulting segmentation is the same as if those elements did not exist. Alternatively, the overlapping elements can be treated as a single element spanning the union of the intersecting parts. Figure 15 depicts these two situations: in the first case, the watermark is considered as part of the background, while in the second, the seal is merged into a single element together with the parts it intersects.

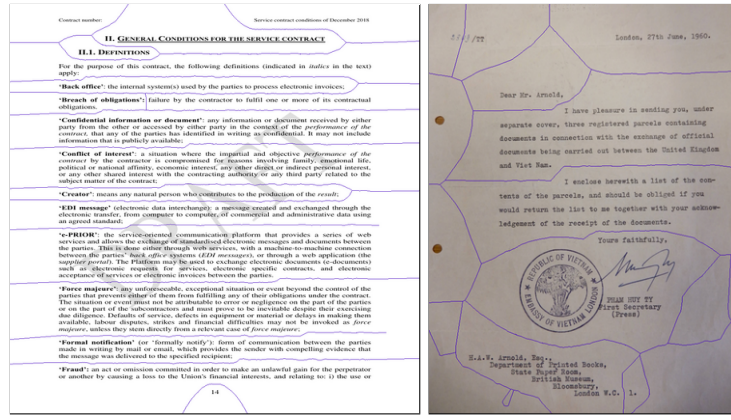


Figure 15: Results on documents with overlapping elements. In the first case, the watermark is considered as part of the background when binarizing the image. Therefore, the segmentation is the same as if it did not exist. In the second case, the seal is considered as a single element together with the other parts it intersects.

**Non-Latin scripts.** Though the method is not explicitly designed for Latin scripts, there are some implicit assumptions that call into question its ability to work on other scripts. It is assumed that characters are, in most cases, a single connected component and that the most frequent spacings are the inter-character spacing and the inter-line spacing. Furthermore, characters in the same font are assumed to have a similar area. This is not the case in every language.

For instance, Arabic or Persian scripts are cursive, meaning that the characters are often connected within a word, the spacing between words and characters is less uniform due to this cursive nature, and the use of diacritics is more prevalent. Three examples of documents in these languages are given in Figure 16. Here we observe that, even if the overall layout is correct, the method struggles to manage diacritics correctly.

Another language that challenges these hypotheses is Korean. Korean characters typically consist of complex, dense structures that are not necessarily connected. The fourth example in Figure 16 shows the result of the method on a Korean document. All in all, the result on this simple layout is satisfactory despite the language's complexities.



Figure 16: Results on documents written in different languages using other than Latin scripts. Note that, even if the results are overall good, the method struggles with the use of diacritics in Arabic and Persian.

**Handwritten text.** Handwritten text presents several unique challenges for document layout analysis that make it significantly more complex than printed text. Unlike printed text, where spacing between characters, words and lines is consistent, handwriting often features irregular spacing, making it more difficult to determine semantically meaningful thresholds  $T_1$  and  $T_2$ . Furthermore, indi-

vidual writing styles such as the use of cursive or ligatures between words and the spacing between punctuation marks and characters may affect the result. Figure 17 shows three examples of the results obtained by the method on handwritten text. In the first two examples we observe that some lines of text as well as some punctuation marks are segmented separately due to the mentioned non-uniformity throughout the text. Note that this problem could also arise in fully justified (not necessarily handwritten) text, as spacing is also non-uniform. On the other hand, the third example shows a satisfactory segmentation, reinforcing the idea that the performance of the method on handwritten documents depends on the specific writing style.

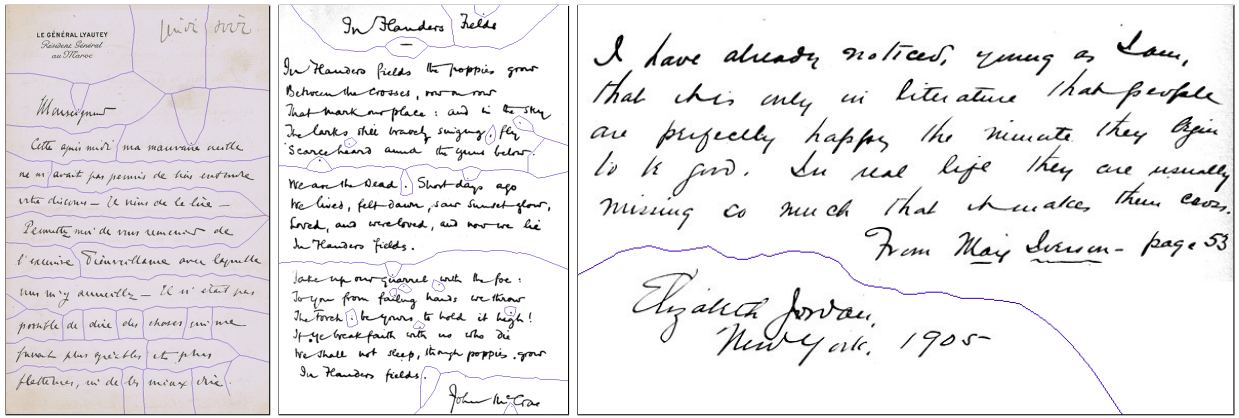


Figure 17: Results on handwritten documents. The performance depends on the particular writing style: while in the first two cases the non-uniform spacing causes a wrong segmentation, in the third example the method achieves a satisfactory result.

## 7 Conclusions

In this work, we presented an efficient and faithful implementation of the method proposed by Kise et al. [8], rigorously testing it across a diverse set of samples. We showed that the method has a reasonable performance in diverse scenarios and is able to handle some complex layouts. Still, we found some inconsistencies in how elements such as lists, drop-caps, and tables are handled, suggesting that the particular styling of each of these can affect the final result.

Furthermore, our experiments revealed a significant sensitivity of the method to parameter settings, with even small adjustments leading to notable changes in the output. Additionally, the method's performance is also affected by the binarization process, highlighting the importance of careful preprocessing even if this step is left unaddressed in the original article.

One key finding is that border sampling, which may seem like a minor detail, has a considerable impact on the final results. This indicates that seemingly peripheral choices in the implementation can alter the method's behavior substantially. Overall, our analysis shows that there is no single set of default parameters that consistently works well across all cases. Effective use of the method requires a context-dependent tuning of parameters.

## Acknowledgments

Work supported by Bpifrance, CollabNext project.

# Image Credits



DocLayNet dataset [11]. License: CDLA-Permissive-1.0.

 Title: *Otro '45 : antología poética*. Publisher: Biblioteca Nacional (Montevideo). License: CC BY 2.0<sup>4</sup>.

 Wikimedia Commons. Author: Leclerc (Philippe François Marie Leclerc de Hauteclocque, dit) (1902-11-22 - 1947-11-28). License: Creative Commons CC0 1.0 Universal Public Domain Dedication<sup>5</sup>.

 Wikimedia Commons. Author: Political Party Fatah. License: Public Domain<sup>6</sup>.

 Wikimedia Commons. Author: Shirali110. License: CC-BY-SA-4.0<sup>7</sup>.

 Wikimedia Commons. Author: Zarbarg. License: CC-BY-SA-4.0<sup>8</sup>.

 Wikimedia Commons. Author: Hubert Lyautey (letter) - Jean-François Miniac (photograph). License: CC BY-SA 3.0<sup>9</sup>.

 Wikimedia Commons. Author: Oliver Brothers. License: Public Domain<sup>10</sup>.

 Wikimedia Commons. Author: Virginia Robie. License: Public Domain<sup>11</sup>.

 Wikimedia Commons. Author: Charlotte Harding. License: Public Domain<sup>12</sup>.

 Wikimedia Commons. Author: John McCrae. License: Public Domain<sup>13</sup>.

## References

- [1] F. AURENHAMMER, *Voronoi Diagrams-A Survey of a Fundamental Geometric Data Structure*, ACM Computing Surveys, 23 (1991), p. 345–405, <https://doi.org/10.1145/116873.116880>.
- [2] A. BANERJEE, S. BISWAS, J. LLADÓS, AND U. PAL, *SwinDocSegmenter: An End-To-End Unified Domain Adaptive Transformer For Document Instance Segmentation*, in International Conference on Document Analysis and Recognition (ICDAR), 2023, pp. 307–325, [https://doi.org/10.1007/978-3-031-41676-7\\_18](https://doi.org/10.1007/978-3-031-41676-7_18).

<sup>4</sup><http://bibliotecadigital.bibna.gub.uy:8080/jspui/bitstream/123456789/132581/4/Otro%2045.pdf>

<sup>5</sup>[https://commons.wikimedia.org/wiki/File:Ordre\\_g%C3%A9n%C3%A9ral\\_n%C2%BD\\_B0\\_88\\_du\\_21\\_juin\\_1945-\\_Citations\\_%C3%A0\\_1%27Ordre\\_de\\_BrigadeR%C3%A9giment,\\_Division,\\_Corps\\_d%C2%BD\\_27Arm%C3%A9e\\_\(Alsace\\_-\\_Allem,\\_2002.2218\(316\).jpg](https://commons.wikimedia.org/wiki/File:Ordre_g%C3%A9n%C3%A9ral_n%C2%BD_B0_88_du_21_juin_1945-_Citations_%C3%A0_1%27Ordre_de_BrigadeR%C3%A9giment,_Division,_Corps_d%C2%BD_27Arm%C3%A9e_(Alsace_-_Allem,_2002.2218(316).jpg)

<sup>6</sup>[https://commons.wikimedia.org/wiki/File:Fatah\\_39\\_January\\_1969.jpg](https://commons.wikimedia.org/wiki/File:Fatah_39_January_1969.jpg)

<sup>7</sup><https://commons.wikimedia.org/wiki/File:Alfeqhalmuqaranp1.jpg>

<sup>8</sup>[https://commons.wikimedia.org/wiki/Category:Documents\\_in\\_Persian#/media/File:IROST-MSRT.jpg](https://commons.wikimedia.org/wiki/Category:Documents_in_Persian#/media/File:IROST-MSRT.jpg)

<sup>9</sup>[https://commons.wikimedia.org/wiki/Category:Handwriting\\_in\\_French#/media/File:Courrier\\_d%27Hubert\\_Lyautey\\_%C3%A0\\_Louis\\_Duchesne,\\_au\\_soir\\_de\\_la\\_r%C3%A9ception\\_de\\_Lyautey\\_%C3%A0\\_1%27Acad%C3%A9mie\\_fran%C3%A7aise\\_en\\_1920,\\_collection\\_Marie-Anne\\_Miniac,\\_Rennes,\\_France..jpg](https://commons.wikimedia.org/wiki/Category:Handwriting_in_French#/media/File:Courrier_d%27Hubert_Lyautey_%C3%A0_Louis_Duchesne,_au_soir_de_la_r%C3%A9ception_de_Lyautey_%C3%A0_1%27Acad%C3%A9mie_fran%C3%A7aise_en_1920,_collection_Marie-Anne_Miniac,_Rennes,_France..jpg)

<sup>10</sup><https://commons.wikimedia.org/wiki/File:Old-brochure-page-one.jpg>

<sup>11</sup>[https://commons.wikimedia.org/wiki/File:Historic\\_styles\\_in\\_furniture\\_\(IA\\_cu31924063909075\).pdf](https://commons.wikimedia.org/wiki/File:Historic_styles_in_furniture_(IA_cu31924063909075).pdf)

<sup>12</sup>[https://commons.wikimedia.org/wiki/File:Handwritten\\_author%27s\\_letter--May\\_Iverson,\\_her\\_story.jpg](https://commons.wikimedia.org/wiki/File:Handwritten_author%27s_letter--May_Iverson,_her_story.jpg)

<sup>13</sup>[https://commons.wikimedia.org/wiki/File:In\\_Flanders\\_fields\\_and\\_other\\_poems,\\_handwritten.png](https://commons.wikimedia.org/wiki/File:In_Flanders_fields_and_other_poems,_handwritten.png)

- [3] A. BANERJEE, S. BISWAS, J. LLADÓS, AND U. PAL, *SemiDocSeg: Harnessing Semi-Supervised Learning for Document Layout Analysis*, International Journal on Document Analysis and Recognition, 27 (2024), p. 317–334, <https://doi.org/10.1007/s10032-024-00473-y>.
- [4] D. CAI, S. YU, J.-R. WEN, AND W.-Y. MA, *VIPS: a Vision-Based Page Segmentation Algorithm*, tech. report, Microsoft Research, 01 2003. <https://www.microsoft.com/en-us/research/wp-content/uploads/2016/02/tr-2003-79.pdf>.
- [5] C. DA, C. LUO, Q. ZHENG, AND C. YAO, *Vision Grid Transformer for Document Layout Analysis*, in IEEE/CVF International Conference on Computer Vision (ICCV), 2023, pp. 19405–19415, <https://doi.org/10.1109/ICCV51070.2023.01783>.
- [6] J. HA, R. HARALICK, AND I. PHILLIPS, *Recursive X-Y Cut Using Bounding Boxes of Connected Components*, in International Conference on Document Analysis and Recognition (ICDAR), vol. 2, 1995, pp. 952–955 vol.2, <https://doi.org/10.1109/ICDAR.1995.602059>.
- [7] Y. ISHIYAMA, C. FUNAOKA, F. KUBO, H. TAKAHASHI, AND F. TOMITA, *Labeling Board Based on Boundary Tracking*, in IAPR International Conference on Pattern Recognition. Vol. IV. Conference D: Architectures for Vision and Pattern Recognition,, 1992, pp. 34–38, <https://doi.org/10.1109/ICPR.1992.202125>.
- [8] K. KISE, A. SATO, AND M. IWATA, *Segmentation of Page Images Using the Area Voronoi Diagram*, Computer Vision and Image Understanding, 70 (1998), pp. 370–382, <https://doi.org/10.1006/cviu.1998.0684>.
- [9] L. O'GORMAN, *The Document Spectrum for Page Layout Analysis*, IEEE Transactions on Pattern Analysis and Machine Intelligence, 15 (1993), pp. 1162–1173, <https://doi.org/10.1109/34.244677>.
- [10] N. OTSU, *A Threshold Selection Method from Gray-Level Histograms*, IEEE Transactions on Systems, Man, and Cybernetics, 9 (1979), pp. 62–66, <https://doi.org/10.1109/TSMC.1979.4310076>.
- [11] B. PFITZMANN, C. AUER, M. DOLFI, A. S. NASSAR, AND P. W. J. STAAR, *DocLayNet: A Large Human-Annotated Dataset for Document-Layout Segmentation*, ACM SIGKDD Conference on Knowledge Discovery and Data Mining, (2022), p. 3743–3751, <https://doi.org/10.1145/3534678.3539043>.
- [12] J. Y. RAMEL, S. LERICHE, M. L. DEMONET, AND S. BUSSON, *User-Driven Page Layout Analysis of Historical Printed Books*, International Journal on Document Analysis and Recognition, 9 (2007), p. 243–261, <https://doi.org/10.1007/s10032-007-0040-6>.
- [13] T. SHEHZADI, D. STRICKER, AND M. Z. AFZAL, *A Hybrid Approach for Document Layout Analysis in Document Images*, ArXiv, (2024), <https://doi.org/10.48550/arXiv.2404.17888>.
- [14] Z. SHEN, R. ZHANG, M. DELL, B. C. G. LEE, J. CARLSON, AND W. LI, *LayoutParser: A Unified Toolkit for Deep Learning Based Document Image Analysis*, in International Conference on Document Analysis and Recognition (ICDAR), 2021, pp. 131–146, [https://doi.org/10.1007/978-3-030-86549-8\\_9](https://doi.org/10.1007/978-3-030-86549-8_9).
- [15] Z. TANG, Z. YANG, G. WANG, Y. FANG, Y. LIU, C. ZHU, M. ZENG, C. ZHANG, AND M. BANSAL, *Unifying Vision, Text, and Layout for Universal Document Processing*, in IEEE/CVF Conference on Computer Vision and Pattern Recognition (CVPR), 2023, pp. 19254–19264, <https://doi.org/10.1109/CVPR52729.2023.01845>.
- [16] X. ZHONG, J. TANG, AND A. JIMENO YEPES, *PubLayNet: Largest Dataset Ever for Document Layout Analysis*, in International Conference on Document Analysis and Recognition (ICDAR), 2019, pp. 1015–1022, <https://doi.org/10.1109/ICDAR.2019.00166>.